Exact analytical solutions in two dimensional plate-like mechanical metamaterials: State of free deformation in a topological cylinder

John T. Klein[a,b], Eduard G. Karpov[a,1]

[a] *University of Illinois at Chicago, Department of Civil and Materials Engineering, 842 W Taylor St, Chicago, IL 60607*
[b] *Oak Ridge Associated Universities Appointment to CCDEVCOM US Army Research Laboratory, Aberdeen Proving Ground, MD 21005*

Abstract

Nodal displacements for two dimensional plate-like lattices under static loading are solved in exact analytical form, when periodic boundary conditions are applied to the top and bottom surfaces of the lattice forming a topological cylinder. Discrete Fourier transform converts the governing equation of static equilibrium into a set of one dimensional wavenumber dependent problems. Characteristic solutions are developed for each Fourier mode of deformation. Inverse discrete Fourier transform converts the wavenumber domain function back to the spatial domain by taking a linear combination of the one dimensional harmonic solutions. As an example, the point force is decomposed into a set of wavenumber dependent loading profiles. A linear combination of the displacement solutions for the individual harmonic loading profiles is sufficient to reproduce the overall displacement solution for the point load. This property holds for any type of the load. Nodal displacements, expressed with analytical dependence on the nodal indices n and m, match the results of commercial finite element analysis software. Overall, this paper demonstrates that the static response of discrete lattices is equivalently represented as a superposition of the wavenumber domain solutions, which is analogous to frequency domain analysis in acoustic metamaterials and phononics.

Keywords:
mechanical metamaterials, lattice mechanics, 2D plate-like lattices, analytical displacement solutions, periodic boundary conditions, discrete Fourier transform

1. Introduction

The field of lattice mechanics seeks to define the static deformation of repetitive structures based on the geometry and elastic properties of a representative sub unit or unit cell [1, 2]. One way of taking this periodicity into account is to express the state of deformation at the current cell recurrently based on the state of deformation of the previous cell. This concept underlies transfer matrix analysis, which was used to study structural wave motion in infinitely periodic structures [3] and later extended to study the elastostatics of finite-length 1D periodic lattices [4, 5] Characteristic solutions were later derived in 1D beam-like trusses, and provided analytical displacement solutions [6]. Figure 1a shows an example of a 1D lattice boundary value problem where displacement solutions were provided in an exact form. Below the lattice is its associate cell, which is defined as the minimal sub structure that captures all mechanical properties of a lattice. Fourier domain methods were formulated to study the mechanics of 1D beam-like and 2D plate-like lattices with periodic boundary conditions [7] as well as 2D and 3D beam lattices with non-periodic boundary conditions [8, 9].

Recently, methods of lattice mechanics facilitated discovery of structures that exhibit unusual mechanical behavior. For instance, highly nonlocal lattices such as the X-braced lattice demonstrate the reversal Saint-Venant's edge effects [10], selective filtering of Fourier harmonics [11] and anomalous strain energy distribution in response to a point load or Gaussian distributed load [12]. Strain energy evolution in these microstructured materials deviates significantly

Email address: ekarpov@uic.edu (Eduard G. Karpov)
[1] Corresponding author

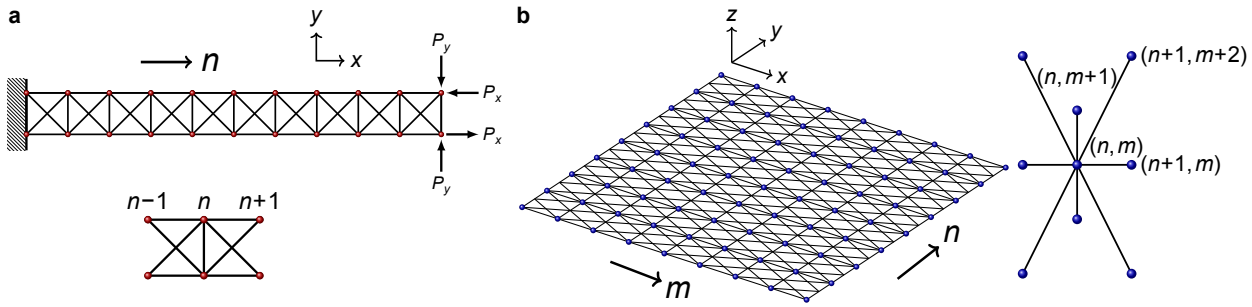

Figure 1: Two types of lattice problems. (a) 1D beam-like X-braced truss from [6]. A single index n describes the periodicity. There are two repeating nodes at each index as shown in the associate cell below. (b) 2D lattice structure from [10]. Indexed by n and m. The associate cell features nearest neighbor and farther nonlocal interactions.

from that of the plane continuum [13] as well as simpler lattices such as hexagonal or square lattices. In this context, there is a clear connection between the study of discrete lattices and the metamaterials paradigm, which states that an unconventional macroscopic response is achieved through the deliberate structuring and collective interactions of smaller structural sub units [14–20].

This paper builds analytical nodal solutions for two dimensional plate-like lattices based on the properties of the repeating sub unit, dimensions of the lattice and force and displacement boundary conditions. The problem is formulated over the periodic rectangular domain for the X-braced lattice, which is identified as a metamaterial structure [10–13]. The spatial displacement solution is obtained by modal decomposition of the static response. In other words, the spatial domain solution is represented as a superposition of wavenumber domain solutions. As an illustrating example, the lattice is subjected to a point load. The corresponding displacement solution to the point load is a summation of wavenumber dependent harmonic sine and cosine functions. Displacements are expressed with analytical dependence on the nodal indices n and m. Analytical results will be shown to agree with high accuracy the results of commercial finite element analysis (FEA) packages such as Abaqus™ or ANSYS™.

2. Problem statement

The X-braced lattice is shown in Figure 2. The associate cell is depicted alongside the lattice. Periodic boundary conditions are applied on the top and bottom nodes. There are eleven nodes in the horizontal direction indexed with integers from $n = 0, 1, \ldots, N$ where $N = 10$. The vertical periodic domain spans $M = 8$ nodes, and is indexed from $m = -4, -3, \ldots, 3$. Periodic boundary conditions require displacements at node (n, m) be equal to displacements at node $(n, m + M)$. The nodal index m represents a discrete periodic sequence that repeats itself after a distance of M nodes. For instance, the responses of bottom nodes along $(n, -4)$ are indistinguishable from the responses of top nodes along $(n, 4)$. The lattice forms a topological cylinder shown on the right of Figure 2.

Example analytical solutions are given for symmetric horizontally applied loads at the left end and a clamped right end, which is the self-equilibrating condition and an interesting problem statement for practical applications of metamaterials as protective or damping layers. This combination of force and displacement boundary conditions also allows for convenient numerical validation of the analytical formulation using commercial finite element analysis (FEA) software such as Abaqus™. Under self-equilibrating conditions the periodic boundary is constrained to move horizontally as denoted by the rollers. Importantly, self-equilibrating loads are not necessary to obtain a closed form of the solution. Only the M-periodicity is required. If loads are asymmetric or not self-equilibrating this creates shear across the X-braced periodic section. The shear strain over the layer can be visualized as torsional strain in the topological cylinder. Rollers at the periodic boundaries would no longer exist. Analytical displacement solutions for non-self equilibrated loading and shear deformation are difficult to validate numerically and thus are not used as examples.

2.1. Equivalent FEA plane problem

The equivalent plane problem is the eleven nodes wide by nine nodes tall structure shown in Figure 2. When applying periodic boundary conditions, the repeating domain is $M = 8$ nodes tall. However, the equivalent FEA

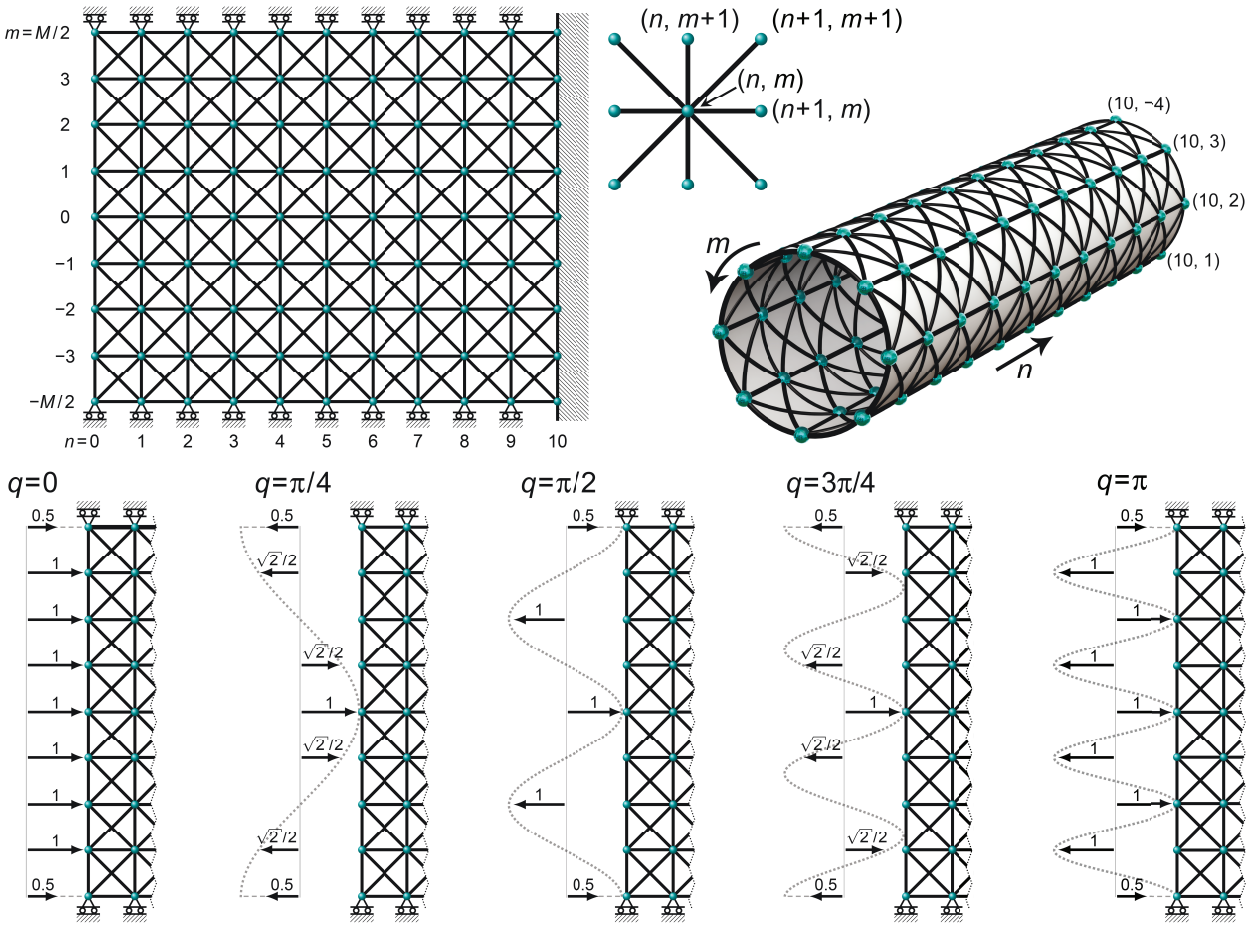

Figure 2: Two dimensional plate-like X-braced lattice. The associate cell is shown to the right of the lattice. Forces are applied on the left end and the right end is clamped. Periodic boundary conditions are applied to top and bottom nodes. Only self-equilibrating loads are considered, which implies periodic boundaries are constrained to move horizontally by the rollers. The response of the top nodes is equivalent to the bottom nodes forming a topological cylinder. Five harmonic loading profiles are shown. The loading profiles and their corresponding analytical displacement solutions are associated with the wavenumber q in the Fourier domain. A linear combination of the loading profiles and their displacement solutions is sufficient to reproduce any type of loading pattern at the surface and any pattern of deformation throughout the lattice.

model is built with nine nodes tall in order preserve symmetry about $m = 0$. To mimic periodic boundary conditions, horizontal bars that connect the nodes along the top and bottom surfaces $(n, 4)$ and $(n, -4)$ are assigned one half of their axial stiffness $\frac{k_1}{2}$ compared to the interior. Loads applied at top and bottom nodes at the left boundary $(0, 4)$ and $(0, -4)$ are halved compared to what they would be in the infinitely periodic problem. Finally, due to the convenience of the analytical formulation the vertical bars along the left boundary $(0, m)$ are assigned one half their axial stiffness $\frac{k_1}{2}$ compared to the interior. The equivalent plane problem yields nodal displacements that are identical to the analytical formulation up to the first five significant figures displayed in Abaqus. As a caveat, the spring element stiffness k in Abaqus must be input as $k = \frac{k_{axial}}{L}$. For example, in the paper the axial stiffness of diagonal bars is $k_2 = 2$. Since the diagonal elements have $\sqrt{2}$ length compared to the vertical and horizontal elements, the spring stiffness entered into Abaqus is $\frac{2}{\sqrt{2}}$. Vertical and horizontal bars are assigned axial stiffness $k_1 = 3$ and length one, which means the spring constant in Abaqus is three.

3. Analysis

3.1. Associate cell

An associate cell is the smallest sub structure needed to define the periodicity and mechanical properties of a lattice. In general, an associate cell consists of a repeating node or group of repeating nodes and all directly interacting elastic connections. Associate cells for triangular and hexagonal honeycomb lattices possess multiple repeating nodes [7]. The X-braced associate cell shown in Figure 2 considers a single repeating node located at (n, m) that is elastically connected to eight adjacent nodes at (n', m'). The nine neighbor connections are decomposed into stiffness blocks $\mathbf{k}$, which are referred to as kernel submatrices. The blocks are associated with bar, beam or solid element stiffness matrices in FEA. In the present analysis, blocks are of dimension 2×2 and are associated with linearly elastic bar element stiffness matrices.

Blocks appear in the two equilibrium equations corresponding to the two nodal degrees of freedom at the current node (n, m). Equilibrium at the current node requires external forces are equal to internal forces

$$\begin{aligned}\mathbf{f}_{nm} = \mathbf{k}_{n-1m-1}\mathbf{u}_{n-1m-1} + \mathbf{k}_{n-1m}\mathbf{u}_{n-1m} + \mathbf{k}_{n-1m+1}\mathbf{u}_{n-1m+1} \\ +\mathbf{k}_{nm-1}\mathbf{u}_{nm} + \mathbf{k}_{nm}\mathbf{u}_{nm} + \mathbf{k}_{nm+1}\mathbf{u}_{nm+1} \\ +\mathbf{k}_{n+1m-1}\mathbf{u}_{n+1m-1} + \mathbf{k}_{n+1m}\mathbf{u}_{n+1m} + \mathbf{k}_{n+1m+1}\mathbf{u}_{n+1m+1}\end{aligned} \tag{1}$$

The above equation states that the mechanical response to an external load applied at (n, m) depends on the state of deformation at the current node (n, m) and the finite region that encompasses its neighbor nodes (n', m'). The equation emphasizes the nonlocality of discrete lattices since there is a direct elastic interaction between the current node and its neighbor nodes separated in space. Far-reaching neighbor interactions may be strong enough to elicit dramatic changes in mechanical properties compared to the continuum [10, 12, 13].

The governing equation of static equilibrium (1) is rewritten as a discrete convolution sum

$$(\mathbf{k} * \mathbf{u})_{nm} = \sum_{n'=n-1}^{n+1} \sum_{m'=m-1}^{m+1} \mathbf{k}_{n-n'm-m'}\mathbf{u}_{n'm'} = \mathbf{f}_{nm} \tag{2}$$

Indices of stiffness blocks are redefined by subtracting neighbor node indices. For example, the diagonal connection between the upper left node and the current node is $\mathbf{k}_{n'm'} = \mathbf{k}_{n-1m+1}$. Block indices are transformed by $\mathbf{k}_{n-n'm-m'} = \mathbf{k}_{n-(n-1)\,m-(m+1)} = \mathbf{k}_{1-1}$. Kernel blocks are defined as

$$\mathbf{k}_{-10} = \mathbf{k}_{10} = k_1 \begin{bmatrix} -1 & 0 \\ 0 & 0 \end{bmatrix} \tag{3a}$$

$$\mathbf{k}_{0-1} = \mathbf{k}_{01} = k_1 \begin{bmatrix} 0 & 0 \\ 0 & -1 \end{bmatrix} \tag{3b}$$

$$\mathbf{k}_{-1-1} = \mathbf{k}_{11} = \frac{k_2}{2\sqrt{2}} \begin{bmatrix} -1 & -1 \\ -1 & -1 \end{bmatrix} \tag{3c}$$

$$\mathbf{k}_{1-1} = \mathbf{k}_{-11} = \frac{k_2}{2\sqrt{2}} \begin{bmatrix} -1 & 1 \\ 1 & -1 \end{bmatrix} \tag{3d}$$

$$\mathbf{k}_{00} = \left(2k_1 + \sqrt{2}k_2\right) \begin{bmatrix} 1 & 0 \\ 0 & 1 \end{bmatrix} \tag{3e}$$

The block $\mathbf{k}_{00} = \mathbf{k}_{nm}$ describes the interaction between the current node and all other nodes in the associate cell and is equal and opposite to the sum of all other blocks. Vertical and horizontal bars have axial stiffness k_1 while diagonal bars have k_2. When $k_1 = k_2$ all bars have equivalent cross-sectional areas and elastic moduli.

3.2. Discrete Fourier transform (DFT)

Periodic boundary conditions in the M-periodic lattice facilitate use of the discrete Fourier transform (DFT). DFT maps the spatial index m to a set of M wavenumbers q in the Fourier domain, $[-\pi, \pi]$. The wavenumber is associated with a vertically distributed harmonic profile of loading or deformation. The governing equation of static equilibrium

(2) is transformed into a set of M one dimensional equilibrium equations where each equilibrium equation is associated with a particular wavenumber

$$\mathbf{F}(n,q) = \mathbf{K}_1(q)\mathbf{U}(n-1,q) + \mathbf{K}_0(q)\mathbf{U}(n,q) + \mathbf{K}_{-1}(q)\mathbf{U}(n+1,q), \quad \text{for all } q = \frac{2\pi\mu}{M}, \;\; \mu = -\frac{M}{2}, \frac{M}{2}+1, \ldots, \frac{M}{2}-1 \tag{4}$$

Here $\mathbf{F}(n,q)$ is the two degree-of-freedom transformed external force vector for the current index n, $\mathbf{K}_1(q)$, $\mathbf{K}_0(q)$, $\mathbf{K}_{-1}(q)$ are the transformed 2×2 stiffness blocks associated with $n-1$, n and $n+1$, respectively and $\mathbf{U}(n-1,q)$, $\mathbf{U}(n,q)$ and $\mathbf{U}(n+1,q)$ are the corresponding transformed two degree-of-freedom displacement vectors. The integer wavenumber index μ denotes the real-valued wavenumber. The discrete Fourier transforms of the displacement and force vectors are defined

$$\mathbf{U}(n,q) = \sum_{m=-M/2}^{M/2-1} \mathbf{u}_{nm} e^{-iqm}, \quad \mathbf{F}(n,q) = \sum_{m=-M/2}^{M/2-1} \mathbf{f}_{nm} e^{-iqm}, \quad \text{for all } q = \frac{2\pi\mu}{M}, \;\; \mu = -\frac{M}{2}, \frac{M}{2}+1, \ldots, \frac{M}{2}-1 \tag{5}$$

The M wavenumber dependent equilibrium equilibrium equations (4) are one dimensional because they are only a function of the horizontal index n. Each one dimensional problem will be solved independently by deriving the characteristic solutions for the wavenumber and then solving for a set of unknown coefficients to satisfy force and displacement boundary conditions. For an M-periodic domain, a linear combination of the M wavenumber dependent solutions is sufficient to reproduce any type of vertically distributed pattern of loading or deformation for a given index n.

Force, stiffness and displacement terms are redefined in the Fourier domain. Transformed stiffness matrices are written as

$$\mathbf{K}_1(q) = \sum_{m=-1}^{1} \mathbf{k}_{1m} e^{-iqm} = \begin{bmatrix} -k_1 - \frac{k_2 \cos q}{\sqrt{2}} & i\frac{k_2 \cos q}{\sqrt{2}} \\ i\frac{k_2 \cos q}{\sqrt{2}} & -\frac{k_2 \cos q}{\sqrt{2}} \end{bmatrix} \tag{6a}$$

$$\mathbf{K}_0(q) = \sum_{m=-1}^{1} \mathbf{k}_{0m} e^{-iqm} = 2\begin{bmatrix} k_1 + \frac{k_2}{\sqrt{2}} & 0 \\ 0 & k_1(1-\cos q) + \frac{k_2}{\sqrt{2}} \end{bmatrix} \tag{6b}$$

$$\mathbf{K}_{-1}(q) = \sum_{m=-1}^{1} \mathbf{k}_{-1m} e^{-iqm} = \mathbf{K}_1(q) \tag{6c}$$

In the interior of the lattice there are no applied external forces

$$\mathbf{F}(n,q) = \mathbf{0} \quad \text{for all interior nodes } n = 1, 2, \ldots, N-1 \tag{7}$$

External force vectors at the left boundary $n = 0$ are transformed

$$\mathbf{F}(0,q) = \sum_{m=-M/2}^{M/2-1} \mathbf{f}_{0m} e^{-iqm} \tag{8}$$

Force vectors $\mathbf{f}_{0m}$ for an arbitrary loading profile, which varies spatially over the vertical m index in the M-periodic domain, are transformed by DFT into a set of M wavenumber dependent vectors $\mathbf{F}(0,q)$. At the right boundary, displacements are fixed. Equilibrium must be satisfied at the two boundaries

$$\text{left boundary:} \quad \mathbf{F}(0,q) = \frac{1}{2}\mathbf{K}_0(q)\mathbf{U}(0,q) + \mathbf{K}_{-1}(q)\mathbf{U}(1,q) \tag{9a}$$

$$\text{right boundary:} \quad \mathbf{U}(N,q) = \mathbf{0} \tag{9b}$$

The equation of equilibrium at the left boundary (9a) is modified from (4) in order to take into account one half of the elastic interactions of the associate cell. In the FEA plane problem, the stiffnesses of the vertical bars along the left boundary are halved relative to interior bars to give an equivalent equilibrium condition as (9a). In the analytical

formulation, the above two equilibrium equations are used to solve for a set of unknown coefficients that impose amplitude and phase changes on the transformed displacement solution. Again to emphasize, arbitrary force and displacement boundary conditions at either end can be used to generate an analytical particular solution. However, the clamped right end and symmetric loading on the left end are convenient in validating the results numerically. The form of the solution is derived from the transfer matrix, which is introduced in the following section.

3.3. Transfer matrix

The transfer matrix $\mathbf{H}$ describes how displacements evolve when moving from one spatial index to the next, see [6]. In the Fourier domain, the transfer matrix specifies how different coarse or fine strain fluctuations defined by the wavenumber decay when moving through the interior of the lattice. The wavenumber dependent transfer matrix arises when considering the transformed governing equation of equilibrium (4) in recurrent form

$$\begin{Bmatrix} \mathbf{U}(n,q) \\ \mathbf{U}(n+1,q) \end{Bmatrix} = \mathbf{H}(q) \begin{Bmatrix} \mathbf{U}(n-1,q) \\ \mathbf{U}(n,q) \end{Bmatrix} \tag{10}$$

The transfer matrix is defined as

$$\mathbf{H}(q) = \begin{bmatrix} \mathbf{0} & \mathbf{I} \\ -\mathbf{K}_{-1}^{-1}(q)\mathbf{K}_1(q) & -\mathbf{K}_{-1}^{-1}(q)\mathbf{K}_0(q) \end{bmatrix} \tag{11}$$

The transfer matrix is dimensionless. It is a property of the associate cell geometry and the stiffnesses of its members. For the X-braced associate cell, the transfer matrix is 4×4. There is a 2×2 zero block on the upper left, 2×2 identity block on the upper right and 2×2 stiffness blocks on the lower left and lower right that describe how the wavenumber dependent displacements evolve when moving horizontally through the lattice. Explicit expressions for the transfer matrix exist for all lattices where an associate cell is defined. More complicated associate cells such as those for more highly nonlocal lattices or even simple hexagonal honeycombs may consider multiple repeating nodes within the index n. The transfer matrices for these associate cells takes into account additional degrees of freedom but still reduces to (11) after applying DFT over the m index.

Displacements are expressed with an explicit dependence on the horizontal index n by exponentiating the transfer matrix in (10) and post multiplying it by the transformation matrix $\mathbf{T}(q)$ and a set of unknown coefficients $\mathbf{C}(q)$

$$\begin{Bmatrix} \mathbf{U}(n,q) \\ \mathbf{U}(n+1,q) \end{Bmatrix} = \mathbf{H}^n(q)\mathbf{T}(q)\mathbf{C}(q) \tag{12}$$

The transformation matrix $\mathbf{T}(q)$ is a 4×4 matrix that stores the eigenvectors of the transfer matrix in its columns. It arises when considering the Jordan decomposition of the transfer matrix (14) and its form (16) will be discussed in the following section. In (12) the transformation matrix scales the unknown coefficients. The product $\mathbf{T}(q)\mathbf{C}(q)$ represents some known initial set of displacements at the boundary. Using (12) it is possible to solve for the four unknown coefficients with the force and displacement boundary conditions at either end. However, exponentiation of the transfer matrix in this form is computationally difficult. Moreover, there are certain wavenumbers that yield a defective transfer matrix. In this case, generalized eigenvectors must be generated in order to give a non-singular transformation matrix and thereby make it possible to solve the lattice boundary value problem. The following section addresses these two issues by introducing a simpler form of the displacement solution in the wavenumber domain.

3.4. Jordan decomposition of the transfer matrix

The transfer matrix $\mathbf{H}(q)$ is decomposed into two parts. The first part is the transformation matrix $\mathbf{T}(q)$ that stores the eigenvectors and the second part is the Jordan matrix $\mathbf{J}(q)$ that stores the eigenvalues. The Jordan decomposition of the transfer matrix then reads

$$\mathbf{H}(q) = \mathbf{T}(q)\mathbf{J}(q)\mathbf{T}^{-1}(q) \tag{13}$$

where from

$$\mathbf{H}^n(q) = \underbrace{\Big(\mathbf{T}(q)\mathbf{J}(q)\mathbf{T}^{-1}(q)\Big)\Big(\mathbf{T}(q)\mathbf{J}(q)\mathbf{T}^{-1}(q)\Big)\ldots}_{n \text{ times}} = \mathbf{T}(q)\mathbf{J}^n(q)\mathbf{T}^{-1}(q) \tag{14}$$

Exponentiation of the transfer matrix is the same as exponentiation of its Jordan form (14). For a deeper discussion of the Jordan canonical form of the transfer matrix see [6]. In this paper, two cases of the Jordan decomposition of the transfer matrix are discussed.

3.5. Unique eigenvalues

The first case is when the transfer matrix for the wavenumber $\mathbf{H}(q)$ gives four unique eigenvalues. Unique eigenvalues come in reciprocal pairs such that $\lambda_1 = 1/\lambda_3$ and $\lambda_2 = 1/\lambda_4$. The geometric multiplicity equals the algebraic multiplicity for every eigenvalue. The Jordan matrix is fully diagonalizable

$$\mathbf{J}^n(q) = \begin{bmatrix} \lambda_1^n(q) & 0 & 0 & 0 \\ 0 & \lambda_2^n(q) & 0 & 0 \\ 0 & 0 & \lambda_3^n(q) & 0 \\ 0 & 0 & 0 & \lambda_4^n(q) \end{bmatrix} \tag{15}$$

Taking the exponent of the diagonal Jordan matrix is the same as taking the exponents of its diagonal elements.

The transformation matrix stores the four linearly independent eigenvectors in its columns

$$\mathbf{T}(q) = \begin{bmatrix} \mathbf{h}_1(q) & \mathbf{h}_2(q) & \mathbf{h}_3(q) & \mathbf{h}_4(q) \\ \mathbf{h}_1(q)\lambda_1(q) & \mathbf{h}_2(q)\lambda_2(q) & \mathbf{h}_3(q)\lambda_3(q) & \mathbf{h}_4(q)\lambda_4(q) \end{bmatrix} \tag{16}$$

Columns in the 4×4 transformation matrix $\mathbf{T}(q)$ are composed of the half eigenvector $\mathbf{h}(q)$ as the first two components and the half eigenvector multiplied by its corresponding eigenvalue as the last two components. For the lattice boundary value problem, four eigenvectors are needed to form a basis since the Hilbert space is four dimensional. For each wavenumber, there are the two equilibrium boundary conditions at either end for the two degrees of freedom giving a total of four equations and four unknown coefficients. However, only the first two components of the eigenvectors (half eigenvectors) are needed to form a solution since there are only two degrees of freedom for a single displacement vector. Physically, the half eigenvectors stored inside the transformation matrix represent specific modes of deformation for the particular wavenumber. These modes of deformation will decay exponentially when moving through the interior of the lattice as a function of the corresponding eigenvalues. This is clarified when deriving the displacement solution (25) and the matrix of characteristic solutions (26).

3.6. Repeated eigenvalues

The second case is when the transfer matrix for the wavenumber $\mathbf{H}(q)$ generates two repeating eigenvalues. The algebraic multiplicity for each eigenvalue is two while the geometric multiplicity is only one. The Jordan matrix is not fully diagonalizable. In this case, the upper triangular Jordan matrix consists of two 2×2 Jordan blocks

$$\mathbf{J}^n(q) = \begin{bmatrix} \lambda_1(q) & 1 & 0 & 0 \\ 0 & \lambda_1(q) & 0 & 0 \\ 0 & 0 & \lambda_2(q) & 1 \\ 0 & 0 & 0 & \lambda_2(q) \end{bmatrix}^n = \begin{bmatrix} \lambda_1^n(q) & n\lambda_1^{n-1}(q) & 0 & 0 \\ 0 & \lambda_1^n(q) & 0 & 0 \\ 0 & 0 & \lambda_2(q)^n & n\lambda_2^{n-1}(q) \\ 0 & 0 & 0 & \lambda_2^n(q) \end{bmatrix} \tag{17}$$

As will be discussed in section 4.2, the special case when $\lambda_1 = \lambda_2 = 1$ for $q = 0$ corresponds to uniform deformation and the Jordan matrix is expressed

$$\mathbf{J}^n(0) = \begin{bmatrix} 1 & n & 0 & 0 \\ 0 & 1 & 0 & 0 \\ 0 & 0 & 1 & n \\ 0 & 0 & 0 & 1 \end{bmatrix} \tag{18}$$

To complete a basis in the transformation matrix $\mathbf{T}(q)$, a generalized eigenvector must be generated for each Jordan block. Generalized eigenvectors must satisfy the Jordan chain condition [6]

$$(\mathbf{H} - \lambda\mathbf{I})\,\mathbf{h}_1 = \mathbf{0}, \;\; (\mathbf{H} - \lambda\mathbf{I})\,\mathbf{h}_2 = \mathbf{h}_1, \ldots, (\mathbf{H} - \lambda\mathbf{I})\,\mathbf{h}_{n_k} = \mathbf{h}_{n_{k-1}} \tag{19}$$

and the orthogonality condition

$$\mathbf{h}_1^T\mathbf{h}_2 = \mathbf{h}_1^T\mathbf{h}_3 = \ldots \mathbf{h}_1^T\mathbf{h}_{n_k} = \mathbf{0} \tag{20}$$

Since there is only one repeating eigenvalue for each block, the dimension of each Jordan block is $n_k = 2$. One generalized eigenvector is needed per block. The transformation matrix for repeating eigenvalues takes the form of (16) except there are two eigenvectors and two generalized eigenvectors in the four columns.

3.7. Characteristic equation

Constructing an explicit expression for the transfer matrix is not necessary in building an analytical solution. The essential ingredients are the eigenvalues and eigenvectors, which describe the decay and types of deformation that occur in the lattice. Associate cell elastic interactions or $\mathbf{k}$ blocks lead to the more fundamental equation

$$\hat{\mathbf{K}} = \sum_n \sum_m \mathbf{k}_{nm} \lambda^{-n} e^{iqm} \tag{21}$$

The matrix $\hat{\mathbf{K}}$ is the result of applying the discrete Fourier transform over the m index to give the wavenumber q, and the discrete Laplace transform over the n index to give the Laplace parameter λ. Mathematically, the eigenvalues are then interpreted as the Laplace parameter. Physically, these eigenvalues are the decay parameters that scale the corresponding modes of deformation when moving through the interior of the lattice.

To determine the eigenvalues and half eigenvectors for a particular wavenumber q requires solving the following equations

$$\det \hat{\mathbf{K}} = 0 \tag{22}$$

$$(\hat{\mathbf{K}} - \lambda \mathbf{I})\mathbf{h} = \mathbf{0} \tag{23}$$

Solving the characteristic polynomial (22) generates the eigenvalues. The system of equations (23) then gives the half eigenvector associated with an eigenvalue. Future studies of three dimensional lattices will incorporate (21) to (23). In this discussion, the analysis focuses on the transfer matrix (11) and its Jordan normal form (14).

3.8. Transformed displacement solution

After determining the Jordan matrix and the transformation matrix for the wavenumber, substitution of (14) into (12) yields

$$\begin{Bmatrix} \mathbf{U}(n,q) \\ \mathbf{U}(n+1,q) \end{Bmatrix} = \mathbf{T}(q)\mathbf{J}^n(q)\mathbf{C}(q) \tag{24}$$

The left hand side stores two sets of displacement vectors. Equation (24) is rewritten to take into account only one displacement vector

$$\mathbf{U}(n,q) = \mathbf{Y}(n,q)\mathbf{C}(q) \tag{25}$$

Equation (25) is the displacement solution for the M one dimensional wavenumber dependent problems. The matrix function $\mathbf{Y}(n,q)$ gives the characteristic solutions for the wavenumber and is defined

$$\mathbf{Y}(n,q) = [\mathbf{T}(q)]_{2\times 4}\, \mathbf{J}^n(q) \tag{26}$$

As discussed, only the first two rows of the transformation matrix $\mathbf{T}(q)$ are needed to generate a single two degree-of-freedom displacement vector $\mathbf{U}(n,q)$. The 4×4 matrix $\mathbf{T}(q)$ in (16) is cut in half so that it considers half eigenvectors $\mathbf{h}(q)$ as the four columns of the matrix $[\mathbf{T}(q)]_{2\times 4}$.

The four unknown coefficients are solved by substituting (25) into boundary conditions (9a) and (9b). After rearranging terms coefficients are expressed as

$$\mathbf{C}(q) = \begin{bmatrix} \frac{1}{2}\mathbf{K}_0(q)\mathbf{Y}(0,q) + \mathbf{K}_{-1}(q)\mathbf{Y}(1,q) \\ \mathbf{Y}(N) \end{bmatrix}^{-1} \begin{Bmatrix} \mathbf{F}(0,q) \\ \mathbf{0} \end{Bmatrix} \tag{27}$$

There are four coefficients since there are two nodal degrees of freedom and two equilibrium equations at either end. In the next section, the M wavenumber dependent solutions $\mathbf{U}(n,q)$ in (25) are recombined to generate the nodal displacement solution in the spatial domain $\mathbf{u}(n,m)$.

3.9. Inverse discrete Fourier transform

The analytical nodal displacement solution $\mathbf{u}(n,m)$ is recovered by a superposition of the M wavenumber dependent solutions through the inverse discrete Fourier transform

$$\mathbf{u}(n,m) = \frac{1}{M}\sum_{\mu=-M/2}^{M/2-1} \mathbf{Y}(n,q)\mathbf{C}(n,q)e^{iqm}, \qquad \text{for all } q = \frac{2\pi\mu}{M},\ \ m = -\frac{M}{2}, \frac{M}{2}+1, \ldots, \frac{M}{2}-1 \tag{28}$$

Since loads and displacements take on discrete values at the nodes, their values are exactly reproduced when transforming from the wavenumber domain back to the spatial domain. This is in contrast to the continuum where in order to exactly reproduce a periodic waveform often requires the superposition of an infinite number of sine and cosine terms in the Fourier series. In the next section, displacement solutions are developed for each wavenumber considered in the $M = 8$ periodic X-braced lattice.

4. Characteristic solutions for the X-braced lattice

The following section begins with the point load applied at the left end of the X-braced lattice. The point load is equivalently expressed as a linear combination of harmonic cosine functions. It follows that if the input point load is decomposed into a set of harmonic force profiles then the overall displacement solution for the point load should be a simple addition of the corresponding displacement solutions for the individual force profiles that make up the point load. This is a property of linear systems and will be demonstrated in the examples.

Five loading conditions are considered in Figure 2. The harmonic load profiles and their corresponding displacement solutions are associated with a particular wavenumber. The matrix of characteristic solutions $\mathbf{Y}(n,q)$ in (26) will be developed for each wavenumber using the Jordan canonical form of the transfer matrix. The $\mathbf{Y}(n,q)$ matrix is composed of half eigenvectors (allowable types of deformation) that are stored in the transformation matrix $[\mathbf{T}(q)]_{2\times4}$ and eigenvalues (decay parameters) that are stored in the Jordan matrix $\mathbf{J}^n(q)$. Force and displacement boundary conditions determine the vector of coefficients $\mathbf{C}(q)$ using (27). The vector scales the characteristic solution matrix to generate the displacement solution for the wavenumber $\mathbf{U}(n,q)$ in (25). The inverse discrete Fourier transform (28) linearly recombines the Fourier domain solutions to form the overall spatial domain displacement solution. As a caveat, Figure 2 shows that loads are halved at the top and bottom periodic boundaries, which is the case for the equivalent FEA plane problem mentioned in Section 2.1. In the present discussion of the analytical DFT formulation loads are not halved. In the examples, the axial stiffness of the horizontal and vertical bars are $k_1 = 3$ and diagonal bars $k_2 = 2$.

The inverse DFT operation (28) is subdivided into three cases for the X-braced M-periodic problem: uniform deformation when $q = 0$, alternating deformation when $q = \pi$ and coarser harmonic modes of deformation when the wavenumber is both positive and negative. In the examples, the periodic domain is $M = 8$ meaning eight evenly spaced wavenumbers are considered in the Fourier domain, $[-\pi, \pi]$. Wavenumber $q = 0$ is represented once. Wavenumber $q = \pi$ is represented once. The remaining wavenumbers come in pairs with opposite signs, $q = \pm 3\pi/4$, $\pm\pi/2$ and $\pm\pi/4$. As will be shown, the component of the solution associated with the positive wavenumber is a complex conjugate to the component associated with the negative wavenumber. Complex conjugates are recombined elegantly by the inverse Fourier transform to form harmonic sine and cosine spatial displacement solutions. In the paper, the asterisk symbol * denotes the scalar, vector or matrix with components replaced by complex conjugates. By definition, the complex conjugate of $x + yi$ is $x - yi$. Complex conjugates have the same sign real component but opposite sign imaginary component.

4.1. Point load

A point load is applied to the middle node $(0, 0)$ at the left side with magnitude $F_0 = 8$ in the horizontal direction. The Kronecker delta δ_{0m} is used to represent a point load (29a). The Kronecker delta equals one when $m = 0$ and equals zero when $m \neq 0$. This means that $\mathbf{f}_{00} = \{8, 0\}^T$ while all other nodal force vectors on the left side are zero.

Starting with this basic expression for the point load the following is derived

$$\mathbf{f}_{0m} = 8\delta_{0m}\begin{Bmatrix}1\\0\end{Bmatrix} \tag{29a}$$

$$= \left(e^{-i\pi m} + e^{-i\frac{3\pi}{4}m} + e^{i\frac{3\pi}{4}m} + e^{-i\frac{\pi}{2}m} + e^{i\frac{\pi}{2}m} + e^{-i\frac{\pi}{4}m} + e^{i\frac{\pi}{4}m} + 1\right)\begin{Bmatrix}1\\0\end{Bmatrix} \tag{29b}$$

$$= \left(\cos m\pi + 2\cos\frac{3m\pi}{4} + 2\cos\frac{m\pi}{2} + 2\cos\frac{m\pi}{4} + 1\right)\begin{Bmatrix}1\\0\end{Bmatrix} \tag{29c}$$

$$= \mathbf{f}_{0m}^{(\pi)} + 2\mathbf{f}_{0m}^{(3\pi/4)} + 2\mathbf{f}_{0m}^{(\pi/2)} + 2\mathbf{f}_{0m}^{(\pi/4)} + \mathbf{f}_{0m}^{(0)} \tag{29d}$$

Performing the discrete Fourier transform over the set of M two degree of freedom input force vectors as in (8) and then taking the inverse transform yields a summation of exponentials (29b). The exponentials are equivalently expressed as harmonic cosine functions with the same wavelength as the associated wavenumber (29c). The functions are the five loading profiles considered in Figure 2. Superposition of the five vector functions in (29d) is plotted in Figure 3. The graph takes a value of eight at $m = 0$ and zero at all other nodes. Loads as well as displacements are discretely defined at the nodes. Outputs to analytical expressions are only meaningful at integer values for the nodal indices n and m. As an aside, an arbitrary set of two degree of freedom force vectors applied on the left end can be represented using exponentials and harmonic functions, which is shown in AppendixA.

The analytical displacement solution for the point load is a linear combination of the displacement solutions associated with the five load profiles in (29d)

$$\mathbf{u}(n,m) = \mathbf{u}(n,m,\pi) + 2\mathbf{u}(n,m,\pm 3\pi/4) + 2\mathbf{u}(n,m,\pm\pi/2) + 2\mathbf{u}(n,m,\pm\pi/4) + \mathbf{u}(n,m,0) \tag{30}$$

This form (30) will be demonstrated in the following sections. Similar to the analytical expression for the point load (29d), the overall displacement solution (30) is reduced to five terms. The plus-minus sign in three of the terms indicates that opposite sign wavenumbers are factored into these components of the displacement solution. Similar to how exponentials in (29b) form cosine functions in (29c) for the input load, there is an analogous redefinition of exponential terms into harmonic sine and cosine functions with the same wavelength as the associated wavenumber for the nodal displacement solution. However, analytical expressions for nodal displacement solutions will be more complicated than those for loading profiles since they are functions of both nodal indices n and m.

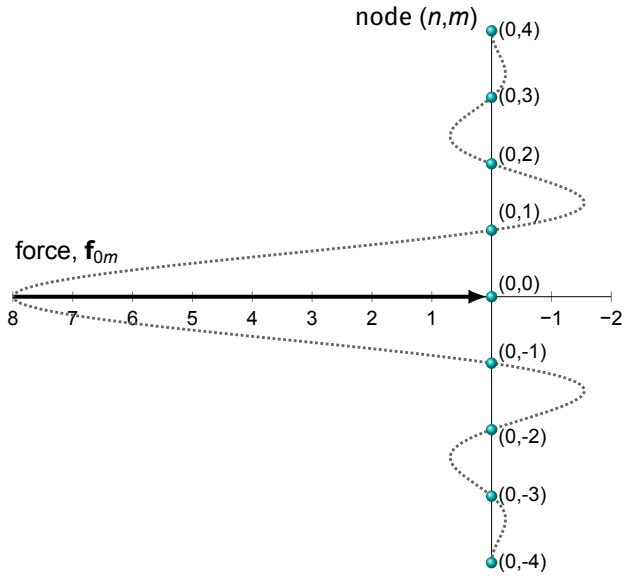

Figure 3: The point load applied at surface nodes $(0, m)$ is represented as a superposition of cosines from (29d). At the middle node $(0, 0)$ the load takes a magnitude of eight while at all other nodes the load is zero. The load is discrete such that the function is only applied to the nodes.

4.2. Uniform deformation

The wavenumber $q = 0$ corresponds to uniform deformation in the horizontal and/or vertical direction. Figure 2 shows a uniform horizontal load applied at the surface. If the lattice is loaded with strictly uniform loads then only characteristic solutions $\mathbf{Y}(n, q)$ corresponding to $q = 0$ will appear in the displacement solution. Jordan decomposition of the transfer matrix associated with this wavenumber reveals there are two sets of repeating eigenvalues equal to one, $\lambda_1 = \lambda_2 = 1$, which is the case (18). Half eigenvectors and the characteristic solution matrix are expressed

$$\mathbf{h}_1 = \begin{Bmatrix} 1 \\ 0 \end{Bmatrix}, \quad \mathbf{h}_2 = \begin{Bmatrix} -1 \\ 0 \end{Bmatrix}, \quad \mathbf{h}_3 = \begin{Bmatrix} 0 \\ 1 \end{Bmatrix}, \quad \mathbf{h}_4 = \begin{Bmatrix} 0 \\ -1 \end{Bmatrix} \tag{31a}$$

$$\mathbf{Y}(n, 0) = \begin{bmatrix} 1 & n-1 & 0 & 0 \\ 0 & 0 & 1 & n-1 \end{bmatrix} \tag{31b}$$

The matrix of characteristic solutions $\mathbf{Y}(n, 0)$ is computed by taking the upper half of the transformation matrix which stores the half eigenvectors and post multiplying it by the Jordan matrix as in (26).

The real-valued coefficients c_1, c_2, c_3 and c_4 stored in the vector $\mathbf{C}(0)$ are found using equilibrium at the boundaries (27). Table 2 shows the values when given amplitude of the uniform horizontal force $F_0 = 1$, axial stiffnesses of the vertical and horizontal bars $k_1 = 3$ and diagonal bars $k_2 = 2$, length of the lattice $N = 10$ and height of periodic domain $M = 8$. The analytical displacement solution for the mode $\mathbf{u}(n, m, q)$ is found by applying the inverse discrete Fourier transform

$$\mathbf{u}(n, m, 0) = \frac{1}{M}\mathbf{Y}(n, 0)\mathbf{C}(0)e^0 = \frac{\sqrt{2}F_0}{k_1\sqrt{2} + k_2}(N - n)\begin{Bmatrix} 1 \\ 0 \end{Bmatrix} \approx \begin{Bmatrix} 2.2654 - 0.22654n \\ 0 \end{Bmatrix} \tag{32}$$

Displacements have first order polynomial dependence on the index n. The above analytical solution matches the FEA simulation in Abaqus. For example, for the vertical set of nodes at $n = 9$ Abaqus outputs a horizontal displacement of $u_x = 0.22654$ and no vertical displacements $u_y = 0$, which agrees with the analytical solution to the five digit significance in Abaqus.

4.3. Alternating load

The wavenumber $q = \pi$ corresponds to loads and deformation that alternate over the M-periodic domain. Figure 2 shows a unit horizontal alternating load at the surface. The Jordan decomposition of the transfer matrix results in a fully diagonalizable Jordan matrix composed of the unique eigenvalues on the diagonal as in (15) and a complete set of eigenvectors stored in the columns of transformation matrix as in (16). Eigenvalues for $k_1 = 3$ and $k_2 = 2$ are shown in Table 1. Half eigenvectors and the form of the characteristic solution matrix are shown

$$\mathbf{h}_1 = \begin{Bmatrix} 1 \\ 0 \end{Bmatrix}, \quad \mathbf{h}_2 = \begin{Bmatrix} 0 \\ -1 \end{Bmatrix}, \quad \mathbf{h}_3 = \begin{Bmatrix} 1 \\ 0 \end{Bmatrix}, \quad \mathbf{h}_4 = \begin{Bmatrix} 0 \\ -1 \end{Bmatrix} \tag{33a}$$

$$\mathbf{Y}(n, \pi) = \begin{bmatrix} \mathbf{h}_1\lambda_1^n & \mathbf{h}_2\lambda_2^n & \mathbf{h}_3\lambda_3^n & \mathbf{h}_4\lambda_4^n \end{bmatrix} \tag{33b}$$

The characteristic solution matrix $\mathbf{Y}(n, \pi)$ stores eigenvalues with an exponential dependence on n. Exponential dependence arises when there are unique eigenvalues.

The unit amplitude alternating load is applied in the horizontal direction at the left end $\mathbf{f}_{0m}^{(\pi)} = \{\cos m\pi, 0\}^T$ and the right boundary is fixed. Unknown coefficients in Table 2 are solved using (27). Inverse DFT gives the spatial displacement solution with analytical dependence on the nodal indices

$$\mathbf{u}(n, m, \pi) = \frac{1}{M}\mathbf{Y}(n, \pi)\mathbf{C}(\pi)e^{i(\pi)m} = \frac{1}{M}\mathbf{h}_1\lambda_1^n c_1 \cos m\pi \approx \begin{Bmatrix} (0.24274)0.18582^n \cos m\pi \\ 0 \end{Bmatrix} \tag{34}$$

The inverse discrete Fourier transform considers all wavenumbers in the summation (28). However, for strictly alternating loads only the $q = \pi$ term appears while all other wavenumber terms have zero coefficient vectors. The exponential term $e^{i(\pi)m} = \cos m\pi$ flips the sign for integer m. For even m the displacement is in the positive direction and for odd m displacement is in the negative direction. Displacements decay exponentially when moving along the index n since $\lambda_1 < 1$. Analytical results are accurate to the five significant figures in Abaqus. For instance, Abaqus outputs +0.24274 at the left boundary nodes $n = 0$ for positive m and −0.24274 for odd m.

4.4. Coarser harmonic modes

Coarser harmonic profiles of deformation are associated with a positive and negative wavenumber. When $M = 8$ these modes correspond to $q = \pm 3\pi/4$, $\pm\pi/2$ and $\pm\pi/4$. Figure 2 shows the three loading profiles associated with these wavenumbers. The choice of axial stiffnesses $k_1 = 3$ and $k_2 = 2$ results in all real-valued eigenvalues in the characteristic solution matrices. Eigenvalues are listed in Table 1. Real-valued eigenvalues allows for elegant recombination of the positive and negative wavenumber components of the spatial domain solution into harmonic sine and cosine functions. When the choice of stiffnesses results in complex-valued eigenvalues the process is similar and is discussed in AppendixB.

Opposite sign wavenumbers $q = -3\pi/4$ and $3\pi/4$ are both considered when taking the discrete Fourier transform for $M = 8$. Transfer matrices associated with these two wavenumbers possess the same four unique eigenvalues. However, their half eigenvectors are complex conjugates. For example, the half eigenvector in the first column of the characteristic solution matrix $\mathbf{Y}(-3\pi/4)$ is $\mathbf{h}_1$. The complex conjugate of $\mathbf{h}_1$ or $\mathbf{h}_1^*$ is associated with the opposite sign wavenumber and stored in the first column of the solution matrix $\mathbf{Y}(3\pi/4) = \mathbf{Y}^*(-3\pi/4)$. The characteristic solution matrix with an asterisk stores identical eigenvalues and complex conjugate half eigenvectors. These relationships hold for the other opposite sign wavenumbers $q = \pm\pi/2$ and $\pm\pi/4$. The forms of the half eigenvectors and characteristic solution matrices for coarser modes of deformation with opposite sign wavenumbers are shown below

$$\mathbf{h}_1 = \begin{Bmatrix} 1 \\ b_1 i \end{Bmatrix}, \quad \mathbf{h}_2 = \begin{Bmatrix} 1 \\ b_2 i \end{Bmatrix}, \quad \mathbf{h}_3 \begin{Bmatrix} 1 \\ -b_1 i \end{Bmatrix}, \quad \mathbf{h}_4 = \begin{Bmatrix} 1 \\ -b_2 i \end{Bmatrix} \tag{35a}$$

$$\mathbf{Y}(n,-q) = \begin{bmatrix} \mathbf{h}_1\lambda_1^n & \mathbf{h}_2\lambda_2^n & \mathbf{h}_3\lambda_3^n & \mathbf{h}_4\lambda_4^n \end{bmatrix}, \quad \mathbf{Y}(n,q) = \mathbf{Y}^*(n,-q) = \begin{bmatrix} \mathbf{h}_1^*\lambda_1^n & \mathbf{h}_2^*\lambda_2^n & \mathbf{h}_3^*\lambda_3^n & \mathbf{h}_4^*\lambda_4^n \end{bmatrix} \tag{35b}$$

Table 2 lists the values of the half eigenvector coefficients b_1 and b_2. The imaginary coefficients are assigned to the negative sign wavenumber and substituted into (35a). Complex conjugate half eigenvectors will have the sign flipped on this imaginary component.

If half eigenvectors are normalized as in (35a) then the coefficient vectors for opposite sign wavenumbers are identical and real-valued

$$\mathbf{C}(-q) = \mathbf{C}(q) = \begin{Bmatrix} c_1 \\ c_2 \\ c_3 \\ c_4 \end{Bmatrix} \tag{36}$$

If opposite sign wavenumbers possess complex conjugate half eigenvectors while their eigenvalues and coefficient vectors are identical then the Fourier domain displacement solutions (25) are also complex conjugates

$$\mathbf{U}(n,-q) = \mathbf{Y}(n,-q)\mathbf{C}(-q), \quad \mathbf{U}(n,q) = \mathbf{U}^*(n,-q) \tag{37}$$

The inverse discrete Fourier transform recombines the positive and negative wavenumber solutions to form the spatial domain displacement solution $\mathbf{u}(n,m,\pm q)$

$$\mathbf{u}(n,m,\pm q) = \frac{1}{M}\left(\mathbf{U}(n,-q)e^{i(-q)m} + \mathbf{U}(n,q)e^{i(q)m}\right) \tag{38a}$$

$$= \frac{1}{M}\begin{Bmatrix} 2\left(c_1\lambda_1^n + c_2\lambda_2^n + c_3\lambda_3^n + c_4\lambda_4^n\right)\cos mq \\ 2\left(b_1c_1\lambda_1^n + b_2c_2\lambda_2^n + b_1c_3\lambda_3^n + b_2c_4\lambda_4^n\right)\sin mq \end{Bmatrix} \tag{38b}$$

The plus-minus sign signifies the spatial domain solution is composed of positive and negative wavenumber parts. Applying the imaginary exponentials and the factor $\frac{1}{M}$, the negative wavenumber part of the spatial displacement solution $\frac{1}{M}\mathbf{U}(n,-q)e^{i(-q)m}$ is the complex conjugate of the positive wavenumber part $\frac{1}{M}\mathbf{U}(n,q)e^{i(q)m}$. Mathematically,

$$\mathrm{Re}\left[\frac{1}{M}\mathbf{U}(n,-q)e^{i(-q)m}\right] = \mathrm{Re}\left[\frac{1}{M}\mathbf{U}(n,q)e^{i(q)m}\right] \tag{39a}$$

$$\mathrm{Im}\left[\frac{1}{M}\mathbf{U}(n,-q)e^{i(-q)m}\right] = -\mathrm{Im}\left[\frac{1}{M}\mathbf{U}(n,q)e^{i(q)m}\right] \tag{39b}$$

When complex conjugates in (38a) are added together the real part is doubled while the imaginary part cancels out. The spatial displacement solution carries no imaginary component. Imaginary exponentials are redefined using Euler's formula. And upon simplification of the expression, the analytical displacement solution is made up of cosine and sine functions (38b) with the same wavelength as the loading profile. Amplitudes depend on the eigenvalues that decay or grow exponentially with the index n and components from the half eigenvectors and coefficients.

Substituting eigenvalues, coefficients and half eigenvector components from Tables 1 and 2 generates analytical solutions that match nodal solutions in Abaqus up to five significant figures. Listed are several nodal displacement solutions computed analytically and then validated using the equivalent FEA plane problem:

- For the $3\pi/4$ wavelength loading profile the analytical formulation yields $\mathbf{u}(1,3) = \{0.0449437, 0.0138783\}^T$. Abaqus outputs $u_x = 0.044943$ and $u_y = 0.013878$.
- For the $\pi/2$ wavelength loading profile the analytical displacement is computed $\mathbf{u}(3,4) = \{0.01429120, 0\}^T$. Abaqus outputs $u_x = 0.014291$ and $u_y = 0$. Another nodal displacement is computed analytically $\mathbf{u}(3,3) = \{0, -0.0067254\}^T$ Abaqus outputs $u_x = 0$ and $u_y = -0.0067254$.
- For the $\pi/4$ wavelength loading profile the analytical solution yields $\mathbf{u}(4,1) = \{0.0641886, 0.0322383\}^T$. The nodal solution in Abaqus is $u_x = 0.064189$ and $u_y = 0.032238$.

Table 1: Eigenvalues associated with each wavenumber

wavenumber	eigenvalues			
q	λ_1	λ_2	λ_3	λ_4
0	1	1	–	–
$\pm\pi/4$	0.52717	0.38022	1.8969	2.6299
$\pm\pi/2$	0.29906	0.10532	3.3437	9.4944
$\pm3\pi/4$	0.20899	−0.044918	4.7847	−22.262
$\pm\pi$	0.18582	−0.096255	5.3814	−10.389

Table 2: Coefficients associated with each wavenumber and half eigenvector components for coarser harmonic modes

wavenumber	coefficients				half eigenvector components	
q	c_1	c_2	c_3	c_4	b_1	b_2
0	16.3109	−1.8123	0	0	–	–
$\pm\pi/4$	-1.2524×10^{-5}	6.5432×10^{-7}	−1.8584	4.3774	1.5781	0.70032
$\pm\pi/2$	−0.92872	2.8760	0	0	−2.0503	−0.66487
$\pm3\pi/4$	−0.20847	2.0076	0	0	−3.9479	−0.41572
$\pm\pi$	1.9419	0	0	0	–	–

4.5. Point load validation

The point load solution matches Abaqus as well. The analytical solution yields $\mathbf{u}(7,3) = \{0.659748, 0.0124928\}^T$. Abaqus outputs $u_x = 0.65974$ and $u_y = 0.012492$. To demonstrate (30), displacements for the node $(2,-3)$ are computed analytically for each of the five displacement profiles and then added together

$$\mathbf{u}(2,-3,\pi) = \{-0.0083822, 0\}^T \tag{40a}$$

$$\mathbf{u}(2,-3,\pm3\pi/4) = \{0.0090988, -0.0021926\}^T \tag{40b}$$

$$\mathbf{u}(2,-3,\pm\pi/2) = \{0, 0.020259\}^T \tag{40c}$$

$$\mathbf{u}(2,-3,\pm\pi/4) = \{-0.19559, -0.064969\}^T \tag{40d}$$

$$\mathbf{u}(2,-3,0) = \{1.8123, 0\}^T \tag{40e}$$

The overall displacement solution for the point load is then

$$\mathbf{u}(2,-3) = \mathbf{u}(2,-3,\pi) + 2\mathbf{u}(2,-3,\pm 3\pi/4) + 2\mathbf{u}(2,-3,\pm\pi/2) + 2\mathbf{u}(2,-3,\pm\pi/4) + \mathbf{u}(2,-3,0) = \begin{Bmatrix} 1.43095 \\ -0.0938036 \end{Bmatrix} \quad (41)$$

Abaqus outputs $u_x = 1.4309$ and $u_y = -0.093803$. The displacement solution for the point load is equivalently represented as a linear combination of the five harmonic patterns of deformation.

5. Conclusion

This investigation presents a powerful technique to solve the two dimensional M-periodic lattice boundary value problem. The algorithm begins by applying the discrete Fourier transform over the governing equation of static equilibrium in order to reduce the two dimensional problem into a set of simpler, tractable M wavenumber dependent one dimensional problems. Characteristic solutions are derived for each problem using basic tools of linear algebra. The spatial domain displacement solution, expressed with analytical dependence on the nodal indices, is recovered by recombining the M wavenumber dependent solutions by the inverse discrete Fourier transform.

The paper reveals that static deformation of a periodic lattice can be decomposed into a set of Fourier mode dependent states of deformation, which are associated with spatially distributed harmonic profiles of loading. The field of metamaterials began as a result of studying optical and acoustic wave propagation in materials and periodic systems. Here, a similar paradigm is adopted except in order to study spatial wave propagation in statically loaded lattices. Therefore, each of optical, acoustic and mechanical metamaterials can be understood in terms of their response to waves. To give an example, there are frequency dependent material properties in acoustics and phononics. Likewise, mechanical properties such as the decay parameters (eigenvalues) depend on the spatial Fourier parameter (wavenumber) in statically loaded lattices, such as in Table 1. If the geometry and stiffnesses parameters of a lattice are changed then this will change the eigenvalues associated with the particular Fourier mode of deformation and thus, alter the rate at which the strain profile decays through the lattice [10, 12]. This is analogous to how the structure and material properties of a lattice affect how different frequencies of sound are transmitted dynamically through its interior.

The algorithm lends itself well to computer automation, and in practice, it is not necessary to display the displacement solution in equation form. However, in understanding that the form of the analytical solution consists of a set of harmonic waves that vary in space, it is now possible to engineer properties of the lattice in order to manipulate how the harmonic functions evolve and thereby control quantities such as the distribution of stresses and strain energy. The problem statement approaches physical loading conditions where loads are applied at one end and the other end is clamped. Analytical nodal solutions are validated using FEA software by setting up an equivalent plane problem. These two facts lend themselves well to future numerical software as well as experimental verification of the metamaterial phenomena projected to occur in 2D plate-like and 3D volumetric lattices. Using these analytical tools, lattices can be properly designed with the right material properties and geometry to achieve new functionalities not seen in traditional continuous materials.

6. Acknowledgements

The authors would like to thank Drs. Thomas A. Plaisted, James M. Sands, and Mark A. Tschopp from the CCDEVCOM Army Research Laboratory for their helpful discussions. This research was sponsored by CCDEVCOM Army Research Laboratory and was accomplished under Cooperative Agreement Number W911NF-18-2-0297. The views and conclusions contained in this document are those of the authors and should not be interpreted as representing the official policies, either expressed or implied, of the Army Research Laboratory or the U.S. Government. The U.S. Government is authorized to reproduce and distribute reprints for Government purposes notwithstanding any copyright notation herein

AppendixA. Representation of an arbitrary distributed load

Any distributed load that spans along a set of repeating nodes can be constructed as a set of harmonic functions. If loads are non-symmetric there will exist phase shifts. Different amplitude sine and cosine functions represent a single

wavelength with a phase shift. For example, if the repeating domain is $M = 8$ then an arbitrary loading profile in the horizontal direction is represented as

$$\begin{aligned}\mathbf{f}_{0m} = \Bigg(&B_4 e^{-i\pi m} + (B_3 + A_3 i)e^{-i\frac{3\pi}{4}m} + (B_3 - A_3 i)e^{i\frac{3\pi}{4}m} \\ &+ (B_2 + A_2 i)e^{-i\frac{\pi}{2}m} + (B_2 - A_2 i)e^{i\frac{\pi}{2}m} + (B_1 + A_1 i)e^{-i\frac{\pi}{4}m} + (B_1 - A_1 i)e^{i\frac{\pi}{4}m} + A_0\Bigg)\begin{Bmatrix}1\\0\end{Bmatrix}\end{aligned} \tag{A.1}$$

$$\begin{aligned}= \Bigg(&B_4 \cos m\pi + 2\left(A_3 \sin\frac{3m\pi}{4} + B_3 \cos\frac{3m\pi}{4}\right) \\ &+ 2\left(A_2 \sin\frac{m\pi}{2} + B_2 \sin\frac{m\pi}{2}\right) + 2\left(A_1 \sin\frac{m\pi}{4} + B_1 \cos\frac{m\pi}{4}\right) + A_0\Bigg)\begin{Bmatrix}1\\0\end{Bmatrix}\end{aligned} \tag{A.2}$$

There are eight coefficients needed to represent eight x-components of the nodal force vectors. The form of the function is the same for the other degree of freedom.

AppendixB. Complex eigenvalues

The choice of axial stiffnesses may result in complex-valued eigenvalues for coarser harmonic modes. Coarser harmonic modes are associated with wavenumbers of opposite sign. As with real-valued eigenvalues, complex eigenvalues are unique and exist in reciprocal pairs $\lambda_1 = 1/\lambda_3$ and $\lambda_2 = 1/\lambda_4$. One distinction of complex eigenvalues is that the pair of eigenvalues whose modulus is less than one are complex conjugates $\lambda_2 = \lambda_1^* \Leftrightarrow \lambda_1 = \lambda_2^*$ and the eigenvalues whose modulus is greater than one are complex conjugates $\lambda_4 = \lambda_3^* \Leftrightarrow \lambda_3 = \lambda_4^*$.

When considering the opposite sign wavenumbers, their eigenvalues are complex conjugates, e.g., the first eigenvalue of the positive wavenumber is a complex conjugate to the first eigenvalue of the negative wavenumber, $\lambda_1(q) = \lambda_1^*(-q)$. It is more useful to write complex eigenvalues in exponential form rather than rectangular form. A complex number in exponential form is the modulus ρ times the imaginary exponential that includes the phase angle ϕ, or $\rho e^{i\phi}$. Eigenvalues associated with the negative wavenumber will have opposite sign phase angles compared to the positive wavenumber but equal modulus. Applying the two identities in the previous paragraph and the relationships between the positive and negative wavenumber lead to (B.1) to (B.2).

The following equations show the forms of the eigenvalues, half eigenvectors, characteristic solution matrices, coefficient vectors and transformed displacement solutions for opposite sign wavenumbers under the scenario when eigenvalues are complex

$$\lambda_1(-q) = \rho e^{-i\phi}, \quad \lambda_2(-q) = \rho e^{i\phi}, \quad \lambda_3(-q) = \rho^{-1} e^{i\phi}, \quad \lambda_4(-q) = \rho^{-1} e^{-i\phi} \tag{B.1}$$

$$\lambda_1(q) = \lambda_1^*(-q) = \rho e^{i\phi}, \quad \lambda_2(q) = \lambda_2^*(-q) = \rho e^{-i\phi}, \quad \lambda_3(q) = \lambda_3^*(-q) = \rho^{-1} e^{-i\phi}, \quad \lambda_4(q) = \lambda_4^*(-q) = \rho^{-1} e^{i\phi} \tag{B.2}$$

$$\mathbf{h}_1 = \begin{Bmatrix}1\\a+bi\end{Bmatrix}, \quad \mathbf{h}_2 = \begin{Bmatrix}1\\-a+bi\end{Bmatrix}, \quad \mathbf{h}_3 \begin{Bmatrix}1\\-a-bi\end{Bmatrix}, \quad \mathbf{h}_4 = \begin{Bmatrix}1\\a-bi\end{Bmatrix} \tag{B.3}$$

$$\mathbf{Y}(n,-q) = \begin{bmatrix}\mathbf{h}_1\lambda_1^n & \mathbf{h}_2\lambda_2^n & \mathbf{h}_3\lambda_3^n & \mathbf{h}_4\lambda_4^n\end{bmatrix}, \quad \mathbf{Y}(n,q) = \mathbf{Y}^*(n,-q) = \begin{bmatrix}\mathbf{h}_1^*\lambda_1^{*n} & \mathbf{h}_2^*\lambda_2^{*n} & \mathbf{h}_3^*\lambda_3^{*n} & \mathbf{h}_4^*\lambda_4^{*n}\end{bmatrix} \tag{B.4}$$

$$\mathbf{C}(-q) = \begin{Bmatrix}c_1 + d_1 i\\ c_1 - d_1 i\\ c_2 + d_2 i\\ c_2 - d_2 i\end{Bmatrix}, \quad \mathbf{C}(q) = \mathbf{C}^*(-q) \tag{B.5}$$

$$\mathbf{U}(n,-q) = \mathbf{Y}(n,-q)\mathbf{C}(-q), \quad \mathbf{U}(n,q) = \mathbf{U}^*(n,-q) \tag{B.6}$$

Opposite sign wavenumbers have complex conjugate eigenvalues, half eigenvectors and coefficient vectors. Thus, their transformed displacement solutions are also complex conjugates. Normalized half eigenvectors and their complex conjugates require only two coefficients a and b. Coefficient vectors are complex. There are only four independent coefficients c_1, c_2, d_1 and d_2 needed to satisfy the boundary conditions at either end.

The combined spatial displacement solution for opposite sign wavenumbers is found by the inverse discrete Fourier transform

$$\mathbf{u}(n,m,\pm q) = \frac{1}{M}\left(\mathbf{U}(n,-q)e^{i(-q)m} + \mathbf{U}(n,q)e^{i(q)m}\right) \tag{B.7}$$

$$\begin{aligned} &= \frac{1}{M}\Big((c_1+d_1i)\mathbf{h}_1\lambda_1^n e^{-iqm} + (c_1-d_1i)\mathbf{h}_1^*\lambda_1^{*n}e^{iqm} + (c_1-d_1i)\mathbf{h}_2\lambda_2^n e^{-iqm} + (c_1+d_1i)\mathbf{h}_2^*\lambda_2^{*n}e^{iqm} \\ &\quad + (c_2+d_2i)\mathbf{h}_3\lambda_3^n e^{-iqm} + (c_2-d_2i)\mathbf{h}_3^*\lambda_3^{*n}e^{iqm} + (c_2-d_2i)\mathbf{h}_4\lambda_4^n e^{-iqm} + (c_2+d_2i)\mathbf{h}_4^*\lambda_4^{*n}e^{iqm}\Big) \end{aligned} \tag{B.8}$$

$$= \frac{1}{M}\begin{Bmatrix} 4\cos mq\Big((c_1\rho^n + c_2\rho^{-n})\cos n\phi + (d_1\rho^n - d_2\rho^{-n})\sin n\phi\Big) \\ 4\sin mq\Big(\big((ad_1+bc_1)\rho^n - (ad_2+bc_2)\rho^{-n}\big)\cos n\phi + \big((bd_1-ac_1)\rho^n - (ac_2-bd_2)\rho^{-n}\big)\sin n\phi\Big) \end{Bmatrix} \tag{B.9}$$

The combined displacement solution for opposite sign wavenumbers will be real-valued. The solution for complex eigenvalues shares relationships to the solution for real eigenvalues (38b).

[1] N. Stephen, P. Wang, On saint-venant's principle in pin-jointed frameworks, International Journal of Solids and Structures 33 (1) (1996) 79–97.

[2] M. Ryvkin, M. Fuchs, B. Nuller, Optimal design of infinite repetitive structures, Structural optimization 18 (2-3) (1999) 202–209.

[3] R. Langley, A transfer matrix analysis of the energetics of structural wave motion and harmonic vibration, Proceedings of the Royal Society of London. Series A: Mathematical, Physical and Engineering Sciences 452 (1950) (1996) 1631–1648.

[4] N. Stephen, P. Wang, On transfer matrix eigenanalysis of pin-jointed frameworks, Computers & Structures 78 (4) (2000) 603–615.

[5] N. Stephen, Transfer matrix analysis of the elastostatics of one-dimensional repetitive structures, Proceedings of the Royal Society A: Mathematical, Physical and Engineering Sciences 462 (2072) (2006) 2245–2270.

[6] E. Karpov, D. Dorofeev, N. Stephen, Characteristic solutions for the statics of repetitive beam-like trusses, International journal of mechanical sciences 44 (7) (2002) 1363–1379.

[7] E. Karpov, N. Stephen, D. Dorofeev, On static analysis of finite repetitive structures by discrete fourier transform, International Journal of Solids and Structures 39 (16) (2002) 4291–4310.

[8] M. Ryvkin, L. Slepyan, Crack in a 2d beam lattice: analytical solutions for two bending modes, Journal of the Mechanics and Physics of Solids 58 (6) (2010) 902–917.

[9] M. Ryvkin, R. Shraga, Fracture toughness of hierarchical self-similar honeycombs, International Journal of Solids and Structures 152 (2018) 151–160.

[10] E. G. Karpov, Structural metamaterials with saint-venant edge effect reversal, Acta Materialia 123 (2017) 245–254.

[11] L. Danso, E. Karpov, Reprogramming static deformation patterns in mechanical metamaterials, Materials 11 (10) (2018) 2050.

[12] E. G. Karpov, L. A. Danso, J. T. Klein, Anomalous strain energy transformation pathways in mechanical metamaterials, Proceedings of the Royal Society A 475 (2226) (2019) 20190041.

[13] E. G. Karpov, L. A. Danso, Strain energy spectral density and information content of materials deformation, International Journal of Mechanical Sciences 148 (2018) 676–683.

[14] M. Kadic, T. Bückmann, N. Stenger, M. Thiel, M. Wegener, On the practicability of pentamode mechanical metamaterials, Applied Physics Letters 100 (19) (2012) 191901.

[15] H. Yasuda, J. Yang, Reentrant origami-based metamaterials with negative poissons ratio and bistability, Physical review letters 114 (18) (2015) 185502.

[16] E. G. Karpov, L. A. Danso, J. T. Klein, Negative extensibility metamaterials: Occurrence and design-space topology, Physical Review E 96 (2) (2017) 023002.

[17] J. T. Klein, E. G. Karpov, Negative extensibility metamaterials: phase diagram calculation, Computational Mechanics 62 (4) (2018) 669–683.

[18] C. Coulais, D. Sounas, A. Alù, Static non-reciprocity in mechanical metamaterials, Nature 542 (2017) 461–464.

[19] T. Frenzel, M. Kadic, M. Wegener, Three-dimensional mechanical metamaterials with a twist, Science 358 (6366) (2017) 1072–1074.

[20] K. Bertoldi, V. Vitelli, J. Christensen, M. van Hecke, Flexible mechanical metamaterials, Nature Reviews Materials 2 (11) (2017) 17066.

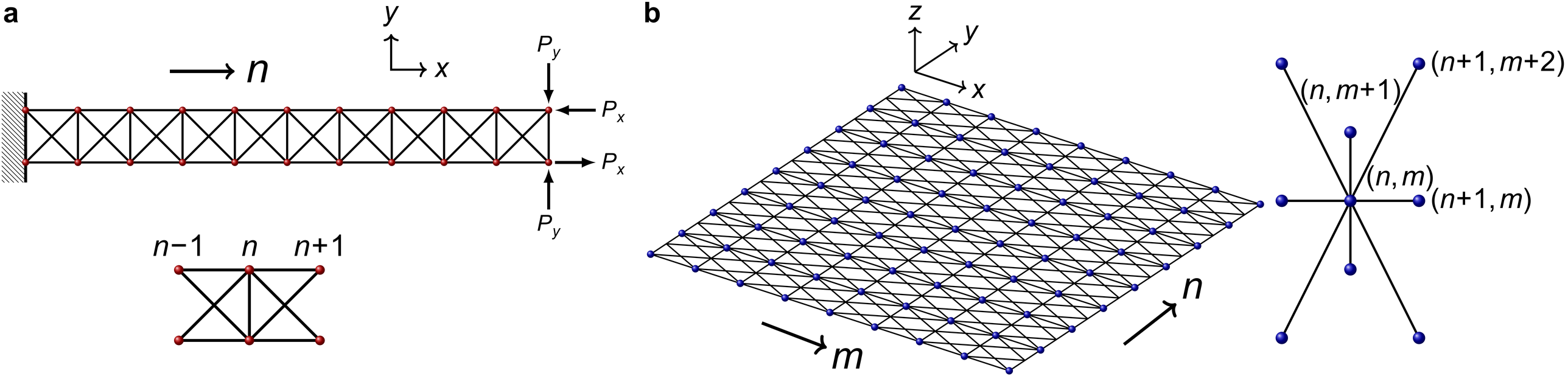
a
y
x
n
P_y
P_x
P_x
P_y
n−1
n
n+1
b
z
y
x
m
n
(n+1, m+2)
(n, m+1)
(n, m)
(n+1, m)

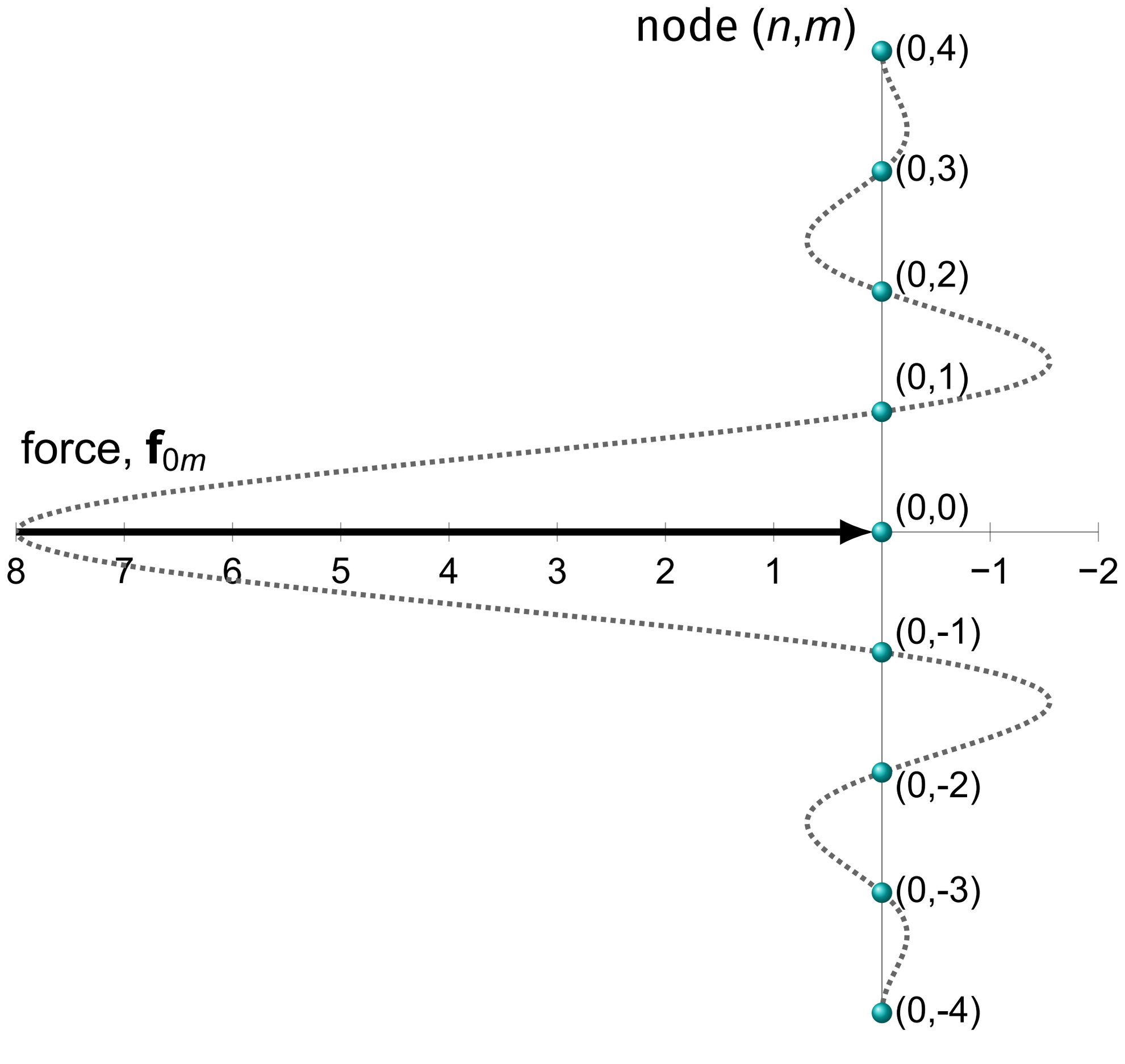
node (n,m)
(0,4)
(0,3)
(0,2)
(0,1)
force, f0m
(0,0)
8
7
6
5
4
3
2
1
−1
−2
(0,-1)
(0,-2)
(0,-3)
(0,-4)

Declaration of interests

 The authors declare that they have no known competing financial interests or personal relationships that could have appeared to influence the work reported in this paper.

☐The authors declare the following financial interests/personal relationships which may be considered as potential competing interests: